A Hybrid Machine Learning Model based on Start-Up Stator Current and High-Resolution Time-Frequency Images for Mechanical Fault Detection and Classification in Induction Motors

Melih Kadir Makara[1], G. Nur Ayas[1], Taner Goktas[1], *Senior Member*, *IEEE*,
and Olcay Akay[1], *Senior Member*, *IEEE*

[1]Department of Electrical and Electronics Engineering
Dokuz Eylul University, Izmir, Turkiye
melihkadir.makara@ogr.deu.edu.tr, ayas.gurcunur@ogr.deu.edu.tr,
taner.goktas@deu.edu.tr, olcay.akay@deu.edu.tr

Abstract

Being one of the backbones of industrial production, induction motors are susceptible to various electrical and mechanical faults which can shorten their lifetime, reduce process efficiency, and increase operational costs. Traditional diagnostics such as vibration, stray-flux, and current analysis require dedicated hardware and expert interpretation although accuracy of those methods may be inconsistent under varying load and speed conditions. Towards overcoming these drawbacks, this study proposes a hybrid machine learning model for fault diagnosis using time - frequency (TF) images derived from start-up stator-current signals. Using start-up transients instead of steady-state signals, we aim to enable fast detection and classification. The proposed convolutional-neural-network (CNN) architecture combines one-dimensional (1D) raw current features with two-dimensional (2D) TF representations to improve accuracy. The approach is implemented in Python via its machine learning libraries. The hybrid model reaches 80.8% classification accuracy, outperforming single-modality CNNs. These findings demonstrate the proposed hybrid model's potential in reliable and effective detection and classification of induction motor faults.

1. Introduction

Induction motors are widely used in industry due to their robust structure, low maintenance requirements, and cost-effective designs. Although induction motors are durable, potential faults should not be overlooked. When a fault happens, it may compromise the safety and reliability of the entire production system. Faults observed in induction motors are generally classified into two main categories: electrical and mechanical. Electrical faults include broken rotor bar and stator short circuited, while mechanical faults comprise misalignment, looseness, imbalance, eccentricity, and bearing faults. According to research, electrical faults constitute 33% to 45% of all motor faults, whereas mechanical faults account for 40% to 53% [1-3]. Various factors such as unsuitable environmental conditions, electrical stress, design and manufacturing defects, overloading, load torque oscillation [4], and overspeed can be attributed to the main causes of faults in induction motors [5].

Undetected faults at an early stage can cause serious problems such as speed and torque fluctuations, temperature rise, insulation issues in stator windings, reduced motor efficiency, and damage to mechanical components including the mounting structure and bearings. These issues can lead to significant financial losses in industry. Therefore, motor condition monitoring and fault diagnosis are critically important to prevent such losses.

Numerous studies exist in the relevant literature for detecting mechanical faults. Motor current signature analysis (MCSA), vibration-based methods, camera-based approaches, stray flux, and thermal analyses are among the most widely used techniques in this field [6]. Research and industrial observations show that vibration-based methods stand out in mechanical fault detection due to their ease of measurement and reliability [7]. However, vibration-based diagnostic approaches have significant limitations such as high sensor costs and the need for expert knowledge [8]. Moreover, mechanical faults like imbalance, looseness, and misalignment typically arise at the rotational frequency, f_r (1X), and its multiples, which makes distinguishing different mechanical fault types difficult [9], [10]. On the other hand, current can be easily obtained through current transformers in protection systems or measured using low-cost and non-invasive converters [11]. Therefore, motor current signal analysis is considered as an effective method for fault diagnosis due to its cost-effectiveness and the advantage of not requiring additional sensors. However, effect of mechanical faults on the current signal presents itself via low-amplitude components, which renders fault detection more challenging [12]. In recent years, hybrid techniques using machine learning and artificial intelligence are employed to overcome these limitations. These recent techniques facilitate the development of reliable and automated fault diagnosis systems [13-15].

In this study, a machine learning-based hybrid fault detection and classification model is proposed based on start-up stator-current data, - not steady state. For this purpose, an experimental ring setup is used [16]. In this setup, misalignment, looseness, and imbalance faults are structurally created in a 5.5 kW induction motor. The proposed hybrid model constitutes time - domain statistics of the start-up stator-current data with time - frequency patterns based on the reassigned spectrogram (RS). The signal is segmented in transient region of the stator current signal and converted into RS images of size 224×224.

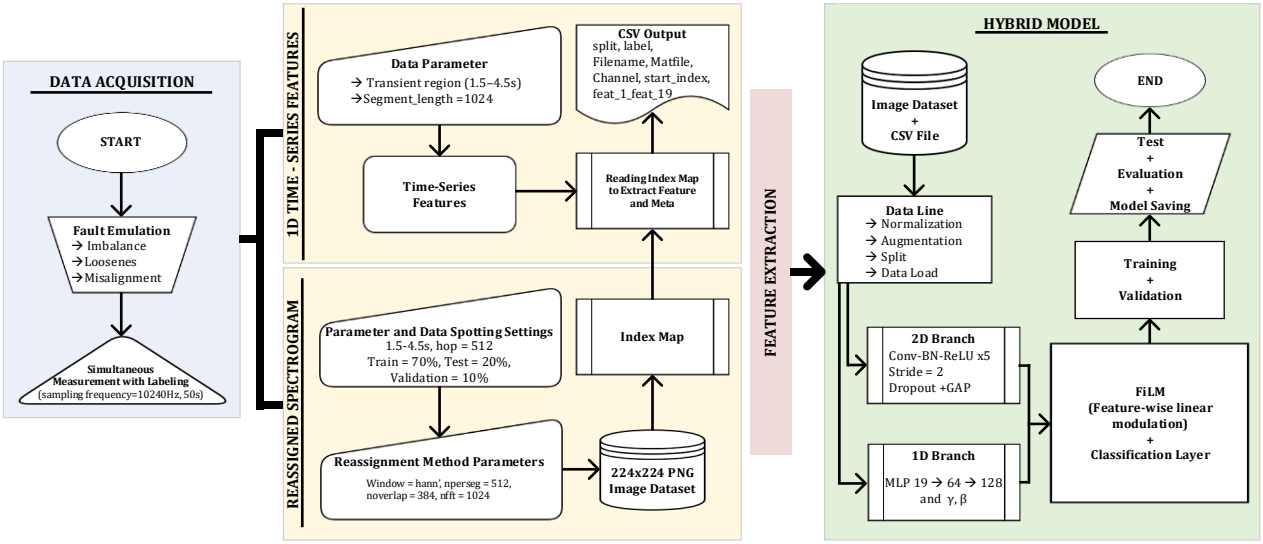

Fig. 1. Proposed hybrid model using startup stator current and high-resolution time - frequency images.

19 statistics are extracted for each segment and mapped to a 2D sample using the file name/starting index. The interaction of the two branches is achieved at the channel level with Feature-wise Linear Modulation (FiLM) in the last two stages of the five-layer CNN. Training is done with Adam optimizer, cosine learning rate scheduler, label smoothing, and masking.

2. Proposed Hybrid Model

The development of the hybrid model consists of three stages. The flow diagram of the proposed hybrid model is illustrated in Fig. 1. The first step is to provide the start-up stator-current data obtained from the test setup as input for both 1D and 2D feature extraction. At the second stage, a 2D RS image dataset is created and an index map file containing segment-index-split mapping for the 1D data is generated. At the third stage, using the index map file 19 time series features are extracted. The 1D features are mapped and saved to a CSV file. Finally, the model is developed and trained using the 1D data and 2D RS images.

2.1. Reassigned Spectrogram (RS) Dataset

The start-up stator-current signal $x[n]$ is converted into RS images. Firstly, the signals are z-normalized and clipped to a range of 1.5 - 4.5 seconds with a sampling frequency of 10.24 kHz. Then, the signals are segmented using the window length of $L = 1024$ and the jump size of $H = 512$, resulting in a total of 1888 samples. The small dataset mainly results from the segmentation process. Data augmentation methods such as time shifting, noise addition, and amplitude scaling are applied to expand it, though excessive augmentation may cause overfitting. Short time Fourier Transform (STFT) analysis employed 50 *msec* Hann windows with 12.5 *msec* hops (75% overlap), and 1024-point spectra providing 10 *Hz* frequency resolution. Since the concepts of STFT analysis and synthesis are fundamental to describing any slowly time - varying signal, the short - time assumption is adopted. Finally, time - frequency reassignment is applied to obtain sharper spectrogram representations. The time and frequency derivatives of the STFT produce the group delay and instantaneous frequency. Using these derivatives, the spectrogram energy is reassigned onto a finer grid resulting in sharper localization of signal components. The reassignment method improves the clarity of the representation by shifting the values away from their starting positions [17]. In spectrograms, the reassignment vector field is directly related to the STFT phase and provides a geometric interpretation used in practice. Reassigned spectrograms are converted into dB scale, cropped to 0 - 2 *kHz*, and stored as 224x224 RGB PNG images. To reduce class imbalance, an equal number of segments are selected per class. The dataset is split into 70%, 20%, and 10%, corresponding to the training, test, and validation subsets, respectively.

2.2. 1D Feature Extraction

The one-phase stator current is segmented between 1.5 - 4.5 *sec* at a sampling frequency of 10.24 *kHz* into non-overlapping windows of 1024 samples or 0.1 *sec*. Each short frame can be assumed to be quasi-stationarity. From each segment, 19 statistical features (RMS, peak, peak-to-peak, skewness, kurtosis, and crest/impulse/clearance/shape factors) are extracted. These features are known to be widely used in rotating machinery diagnostics [18]. Segment identifiers (labels and splits) are not regenerated but directly imported from the previously created 2D image logs. This approach ensures a one-to-one correspondence between 1D features and 2D samples while minimizing the risk of data leakage. The resulting feature table, stored together with metadata (*file name, channel, start index*), is fed as input to the hybrid classifier.

2.3 Hybrid Model Architecture

Single-model CNNs that learn only from RS images are prone to overfitting and poor generalization, especially under limited data, varying speed/load conditions, and noise. Moreover, they may fail to capture critical clues when spectral patterns become ambiguous [19]. When used together, 1D statistics and 2D time - frequency maps together provide more stable and accurate results than employing a single CNN. This complementary use enables the capture of both amplitude/statistical anomalies and harmonic/sideband signatures [20].

This work implements a hybrid pipeline that combines 1D time - series statistics and 2D RS images with feature-level early fusion. Streams are segmented in the range of 1.5 - 4.5 *sec*; 19 time - domain features are z-normalized only by the training set statistics, and each segment is mapped into a 224×224 RGB RS image. SpecAugment is applied to decrease overfitting of the model to narrow-band clue by randomly masking time and frequency bands in the RS images. The 2D branch reduces the size of the RS images from 224 to 7 using five Convolution - Batch Normalization - Rectified Linear Unit (Conv – BN - ReLU) blocks with stride of 2, producing a 256-dimensional representation after global average pooling.

The 1D branch uses a 19 - 64 - 128 Multi-Layer Perceptron (MLP) to form a summary representation. It also produces FiLM coefficients, (γ, β). These coefficients condition the 2D feature maps in the Conv4 - Conv5 layers. The modulation is applied after batch normalization and before ReLU using channel-wise affine transformation. FiLM utilizes 1D statistics to amplify or suppress time - frequency channels in a sample-dependent manner [21]. This enables a more consistent, interpretable, and data-efficient fusion guided by 1D context, particularly for ambiguous RS patterns. The classifier head follows a 256 - 64 - 4 layout. It is optimized using cross-entropy and label smoothing. This reduces overfitting and improves probability calibration. The model uses Adam optimizer and cosine annealing for balanced, efficient updates [22]. Dropout, gradient clipping, and a light L2 penalty on the 1D branch are applied. Evaluation includes test-set accuracy, per-class precision, recall, F1 score, confusion matrices, and one-vs-rest receiver operating characteristic - area under curve (ROC - AUC).

3. Test Ring Setup and Results

3.1. Test Ring Setup

In order to test the proposed hybrid machine learning-based fault detection and classification model, an experimental setup consisting of an induction motor and a DC generator is used [16]. The tested motor is 380 *V*, 5.5 *kW*, 60 *Hz*, 4-pole, and 1800 *rpm*. The load is controlled at 0%, 50%, 75%, and 100% rated load levels by adjusting the field voltage of the 30 *kW* DC generator connected to the test motor. A laser alignment tool is used to align the test motor with the load, where the alignment error is maintained below 0.1 *mm* in vertical and horizontal directions except for the misalignment testing. Under the motor starting condition, the measured three-phase line currents are collected for 50 *sec* at a sampling frequency of 10.24 *kHz*. The collected start-up stator-current data is used as the input of the proposed hybrid model.

Three different mechanical faults are created on the test setup. The imbalance fault is generated by attaching a 3 *mm* thick aluminum disk to the shaft and adding a 33 *g* steel bolt at a radius of 243 *mm* from the shaft center. To produce misalignment fault, a 1.0 *mm* shim is added to the non-driven end of the motor. The structural looseness fault is induced by loosening the four mounting bolts of the motor by 1 *mm* in height.

3.2. Results

Fig. 2 shows the STFT-based RSs of start-up stator-current signals for different fault conditions: imbalance (Fig. 2a), looseness (Fig. 2b), and misalignment (Fig. 2c). As observed in Fig. 2, all fault conditions exhibit strong components in the lower frequency bands, indicating the presence of specific harmonics. However, distinguishing between the three different fault conditions based only on visual analysis of the RSs is challenging. The overall patterns are highly analogous and distinct fault signatures are not visually apparent. The red-colored high energy components representing the sidebands and harmonics of the supply frequency are not horizontal. In some faults, the energy of those sidebands and harmonics is high, while in others it is somewhat low.

The lack of steady-state characteristics in the start-up data causes distortions in the RS images, which negatively affects the classification performance. Therefore, to improve classification performance, a hybrid model is designed using both RS images of faults and 1D time features. The hybrid model is trained and validated. After the model is trained and validated, the model's best weights are recorded. This recorded model is then reloaded and tested using the test data. As presented in Table 1, the proposed hybrid model achieves a test accuracy of 80.8%. The other results in the same table show that this performance significantly surpasses the tested 2D CNN models, including the Residual-CNN model, on the same dataset. Compared to the other models in Table 1, the hybrid model requires more epochs due to its hyperparameter sensitivity, which prolongs its training time. 1888 data samples in total are used for model training. While this data size is insufficient for most models, it is sufficient for the hybrid model. In addition, the risk of overfitting is very high in models trained with small data sets. Efforts to prevent overfitting often fail to prevent the negative consequences of insufficient data.

Accuracy is calculated by calculating the ratio of correctly predicted data to the number of total data set. However, this metric is not always sufficient for multiple classification problems. Precision measures the proportion of a model's positive predictions as true positives. Recall indicates the extent to which a model captures true positives. These measures and F1-score are displayed in Table 2 which shows that healthy (fault-free) data are rarely classified as faulty. This means that the model can distinguish the healthy class reliably. For the imbalance class, the precision value is lower than that of the healthy class. In other words, every time the model makes an imbalance decision, 23% of these decisions are incorrect. Furthermore, based on the recall value, it can be said that the model misses 21% of the true imbalance data. The success rate for the looseness class in terms of model accuracy is 95%, although it can also be observed that 22% of the looseness data is wrongly classified. According to the recall value, the model correctly predicts most of the true misalignment examples. However, based on precision value, we can state that 29% of the data the model identifies as misalignment belong to a different class.

Table 1. Model comparison

Model	Feature Layers	Test Accuracy (%)	Train Duration (mins)
Hybrid Model	2D CNN+1D MLP	80.8	132
Resnet-18	2D CNN	34.2	55
EfficientNet B0	2D CNN	27.6	49
MobileNet V2	2D CNN	58.1	44
Simple-CNN Model	2D CNN	39.2	48
Residual-CNN Model	2D CNN	54.7	63

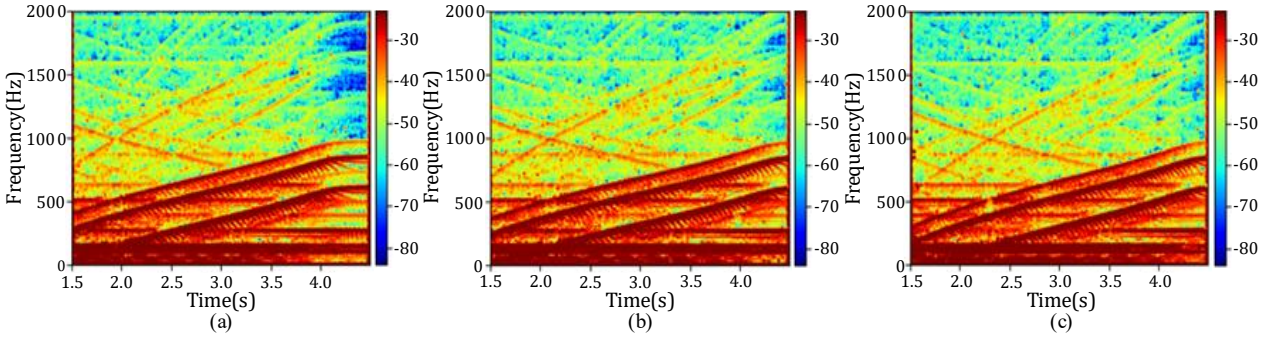

Fig. 2. STFT-based reassigned spectrograms of start-up stator-current signals; (a) imbalance, (b) looseness, (c) misalignment

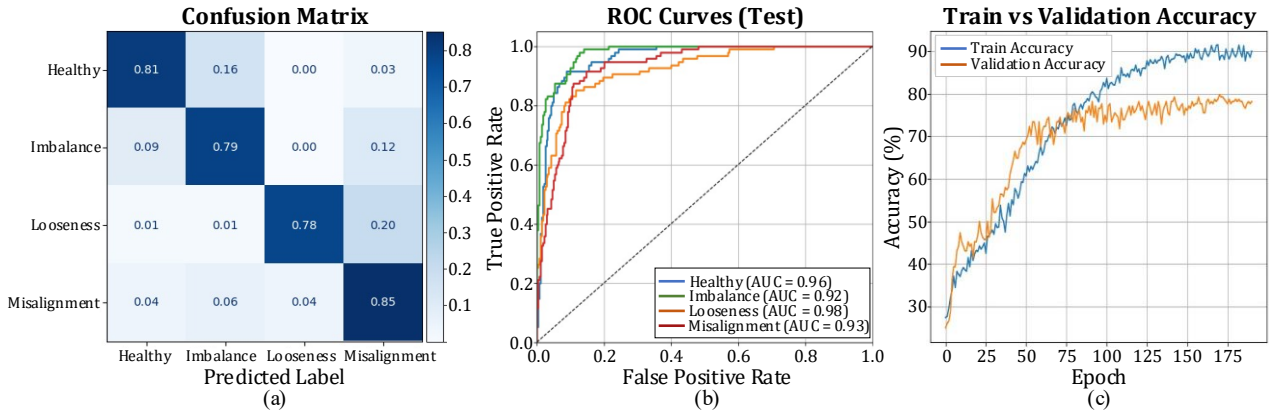

Fig. 3. Performance evaluation visualizations
(a) Confusion matrix, (b) ROC curves and AUC values, (c) Train and validation accuracy curves

Table 2. Performance of the hybrid model for different fault types

	Precision	Recall	F1-Score
Healthy	0.85	0.81	0.83
Imbalance	0.77	0.79	0.78
Looseness	0.95	0.78	0.86
Misalignment	0.71	0.85	0.78

The confusion matrix presented in Fig. 3a separates the number of ground truth examples for each class from the number of predicted examples. In other words, the values in this matrix represent recall. This provides a clear visualization of the model's classification performance, indicating that the model predicts the classes accurately. As shown in Fig. 3b, the ROC curves, located near the upper-left corner with AUC values ranging from 0.92 to 0.98, confirm the model's strong classification performance. Fig. 3c shows the train and validation curves, illustrating how the accuracies of both increase with the number of epochs. However, while the training accuracy continues to increase between 75 and 100 epochs, the validation accuracy remains stable, indicating some overfitting. A major cause of overfitting is insufficient data; in this case, each class contains 95 examples due to the 3-sec transient and the window size limitation applied to maintain data quality. To further mitigate overfitting, processes such as 1D – 2D one-to-one matching, equal segment allocation for class balancing, normalization, augmentation, L2 regularization, dropout, and label smoothing might be employed.

4. Conclusions

This study presented a novel hybrid 1D + 2D fusion model for diagnosing mechanical faults in induction motors using start-up stator-current signals. The proposed approach effectively combines 1D statistical features with 2D time - frequency representations through FiLM-based modulation, addressing the limitations of conventional 2D CNNs.

The results show that the model achieved 80.8% accuracy in testing, with macro-F1-score of 0.81 and AUC values of 0.92 through 0.98, with error density occurring primarily in the imbalance-misalignment faults. Additionally, the proposed hybrid model achieves an F1-score of more than 80% for healthy and looseness classes and an F1-score of 78% for both imbalance and misalignment classes.

In conclusion, the findings demonstrate that the proposed hybrid approach provides more stable and effective fault diagnosis compared to 2D Convolutional Neural Networks (2D CNNs). Using 1D start-up current data together with 2D RS images in the model increases performance. This allows for more accurate detection of difficult-to-diagnose start-up fault characteristics. Consequently, the proposed hybrid model presents a robust and reliable diagnostic tool for practical industrial applications.

In future studies, the real - time pipeline triggered at start-up and running at the edge (STFT/RS + 1D + 2D inference) will be validated and the stability of the PLC/HMI integration will be evaluated.

5. Appendix

All current measurements for imbalance, misalignment, and looseness fault conditions can be downloaded from https://home.eecs.korea.ac.kr/publications/database.

The operating conditions include 60-*Hz* direct online, 20, 40, and 60-*Hz* inverter-fed sources and 0%, 50%, 75%, and 100% load.

6. References

[1] A. H. Bonnett, "Root cause failure analysis for AC induction motors in the petroleum and chemical industry," *Record of Conference Papers, Industry Applications Society, 57th Annual Petroleum and Chemical Industry Conference (PCIC)*, San Antonio, TX, USA, 2010, pp. 1-13, doi: 10.1109/PCIC.2010.5666831.

[2] Report of large motor reliability survey of industrial and commercial installations, Part I," in *IEEE Transactions on Industry Applications*, vol. IA-21, no. 4, pp. 853-864, July 1985, doi: 10.1109/TIA.1985.349532.

[3] Y. L. Karnavas, I. D. Chasiotis, M. Drakaki and I. A. Tziafettas, "Recent advances of neural network-based methods in induction motor fault diagnosis," *2020 International Conference on Electrical Machines (ICEM)*, Gothenburg, Sweden, 2020, pp. 1411-1417, doi: 10.1109/ICEM49940.2020.9270873.

[4] T. Goktas, M. Arkan, M. Zafarani and B. Akin, "Separation harmonics for detecting broken bar fault in case of load torque oscillation," *2015 IEEE International Electric Machines & Drives Conference (IEMDC)*, Coeur d'Alene, ID, USA, 2015, pp. 1452-1458, doi: 10.1109/IEMDC.2015.7409253.

[5] C. Jiang, S. Li, and T. G. Habetler, "A review of condition monitoring of induction motors based on stray flux," *2017 IEEE Energy Conversion Congress and Exposition (ECCE),* Cincinnati, OH, USA, 2017, pp. 5424–5430, doi: 10.1109/ECCE.2017.8096907.

[6] R. Jigyasu, A. Sharma, L. Mathew and S. Chatterji, "A review of condition monitoring and fault diagnosis methods for induction motor," *2018 Second International Conference on Intelligent Computing and Control Systems (ICICCS)*, Madurai, India, 2018, pp. 1713-1721, doi: 10.1109/ICCONS.2018.8662833.

[7] L. Guo, Y. Lei, S. Xing, T. Yan and N. Li, "Deep convolutional transfer learning network: A new method for intelligent fault diagnosis of machines with unlabeled data," in *IEEE Transactions on Industrial Electronics*, vol. 66, no. 9, pp. 7316-7325, Sept. 2019, doi: 10.1109/TIE.2018.2877090.

[8] X. Chen, W. Xu, Y. Liu and M. R. Islam, "Bearing corrosion failure diagnosis of doubly fed induction generator in wind turbines based on stator current analysis," in *IEEE Transactions on Industrial Electronics*, vol. 67, no. 5, pp. 3419-3430, May 2020, doi: 10.1109/TIE.2019.2917418.

[9] B. Battulga, M. F. Shaikh, T. Goktas, M. Arkan and S. B. Lee, "Vibration-based detection and classification of mechanical defects in induction motor-driven systems during the starting transient," in *IEEE Transactions on Industry Applications*, vol. 61, no. 5, pp. 6994-7003, Sept.-Oct. 2025, doi: 10.1109/TIA.2025.3554469.

[10] Technical Associates of Charlotte, P.C. "Illustrated Vibration Diagnostic Chart," R-0894-4, 1996.

[11] V. Aviña-Corral, J. Rangel-Magdaleno, C. Morales-Perez and J. Hernandez, "Bearing fault detection in adjustable speed drive-powered induction machine by using motor current signature analysis and goodness-of-fit tests," in IEEE Transactions on Industrial Informatics, vol. 17, no. 12, pp. 8265-8274, Dec. 2021, doi: 10.1109/TII.2021.3061555

[12] M. Sun, H. Wang, P. Liu, Z. Long, J. Yang and S. Huang, "A novel data-driven mechanical fault diagnosis method for induction motors using stator current signals," in *IEEE Transactions on Transportation Electrification*, vol. 9, no. 1, pp. 347-358, March 2023, doi: 10.1109/TTE.2022.3163612

[13] M. -Q. Tran, M. -K. Liu, Q. -V. Tran and T. -K. Nguyen, "Effective fault diagnosis based on wavelet and convolutional attention neural network for induction motors," in *IEEE Transactions on Instrumentation and Measurement*, vol. 71, pp. 1-13, 2022, Art no. 3501613, doi: 10.1109/TIM.2021.3139706.

[14] M. Z. Ali, M. N. S. K. Shabbir, S. M. K. Zaman and X. Liang, "Machine learning based fault diagnosis for single- and multi-faults for induction motors fed by variable frequency drives," *2019 IEEE Industry Applications Society Annual Meeting*, Baltimore, MD, USA, 2019, pp. 1-14, doi: 10.1109/IAS.2019.8912395.

[15] M. Z. Ali, M. N. S. K. Shabbir, X. Liang, Y. Zhang and T. Hu, "Machine learning-based fault diagnosis for single-and-multi-faults in induction motors using measured stator currents and vibration signals," in *IEEE Transactions on Industry Applications,* vol. 55, no. 3, pp. 2378-2391, May-June 2019, doi: 10.1109/TIA.2019.2895797.

[16] B. Battulga, M. F. Shaikh, J. W. Chun, S. B. Park, S. S. and S. B. Lee, "MEMS accelerometer and hall sensor-based identification of electrical and mechanical defects in induction motors and driven systems," in *IEEE Sensors Journal*, vol. 24, no. 19, pp. 31104-31113, 1 Oct.1, 2024, doi: 10.1109/JSEN.2024.3447869.

[17] F. Auger and P. Flandrin, "Improving readability of time-frequency and time scale representations by reassignment", *IEEE Transactions on Signal Processing,* vol. 43, issue 5, pp. 1068-1089, May 1995, doi: 10.1109/78.382394.

[18] M. Sun, H. Wang, P. Liu, Z. Long, J. Yang, S. Huang, "A novel data-driven mechanical fault diagnosis method for induction motors using stator current signals*," IEEE Trans. Transportation Electrification*, vol. 9, no. 1, pp. 347–358, 2023. doi: 10.1109/TTE.2022.3163612.

[19] M. Zhao, S. Zhong, X. Fu, B. Tang, and M. Pecht, "Deep residual shrinkage networks for fault diagnosis," *IEEE Transactions on Industrial Informatics*, vol. 16, no. 7, pp. 4681–4690, 2020, doi: 10.1109/TII.2019.2943898.

[20] J. Wang, X. Ma, H. Lin, and Z. Chen, "A light weight multisensory fusion model for induction motor fault diagnosis," *IEEE/ASME Transactions on Mechatronics*, 2023, doi: 10.1109/TMECH.2022.3169143.

[21] E. Perez, F. Strub, H. de Vries, V. Dumoulin, A. Courville, "FiLM: Visual reasoning with a general conditioning layer," Proc. ICLR, 2018.

[22] M. T. Koçyiğit, T. M. Hospedales and H. Bilen, "Accelerating self-supervised learning through efficient training strategies," *2023 IEEE/CVF Winter Conference on Applications of Computer Vision (WACV)*, Waikoloa, HI, USA, 2023, pp. 5643-5653, doi: 10.1109/WACV56688.2023.00561.